

# Shape Distribution Matters: Shape-specific Mixture-of-Experts for Amodal Segmentation under Diverse Occlusions

Zhixuan Li<sup>1</sup>, Yujia Liu<sup>2,3,4</sup>, Chen Hui<sup>5</sup>, Jeonghaeng Lee<sup>6</sup>, Sanghoon Lee<sup>6</sup>, Weisi Lin<sup>1\*</sup>

<sup>1</sup>College of Computing and Data Science, Nanyang Technological University, Singapore

<sup>2</sup>School of Computer Science, Peking University, Beijing, China

<sup>3</sup>National Key Laboratory for Multimedia Information Processing, Peking University, Beijing, China

<sup>4</sup>National Engineering Research Center of Visual Technology, Peking University, Beijing, China

<sup>5</sup>Nanjing University of Information Science and Technology, China

<sup>6</sup>Department of Electrical and Electronic Engineering, Yonsei University, Korea

## Abstract

Amodal segmentation targets to predict complete object masks, covering both visible and occluded regions. This task poses significant challenges due to complex occlusions and extreme shape variation, from rigid furniture to highly deformable clothing. Existing one-size-fits-all approaches rely on a single model to handle all shape types, struggling to capture and reason about diverse amodal shapes due to limited representation capacity. A natural solution is to adopt a Mixture-of-Experts (MoE) framework, assigning experts to different shape patterns. However, naively applying MoE without considering the object’s underlying shape distribution can lead to mismatched expert routing and insufficient expert specialization, resulting in redundant or underutilized experts. To deal with these issues, we introduce ShapeMoE, a shape-specific sparse Mixture-of-Experts framework for amodal segmentation. The key idea is to learn a latent shape distribution space and dynamically route each object to a lightweight expert tailored to its shape characteristics. Specifically, ShapeMoE encodes each object into a compact Gaussian embedding that captures key shape characteristics. A Shape-Aware Sparse Router then maps the object to the most suitable expert, enabling precise and efficient shape-aware expert routing. Each expert is designed as lightweight and specialized in predicting occluded regions for specific shape patterns. ShapeMoE offers well interpretability via clear shape-to-expert correspondence, while maintaining high capacity and efficiency. Experiments on COCOA-cls, KINS, and D2SA show that ShapeMoE consistently outperforms state-of-the-art methods, especially in occluded region segmentation. The code will be released.

## 1 Introduction

Amodal instance segmentation (Li and Malik 2016) aims to predict complete object masks, including occluded regions. A key challenge lies in the wide variation of complete object shapes, making accurate segmentation under occlusion particularly difficult. Specifically, some objects exhibit rigid and regular geometries, while others present highly deformable and irregular structures. Such high variation in shape introduces significant complexity to the learning process. Amodal segmentation has broad real-world ap-

plicability (Lee, Jeon, and Le 2023; Follmann et al. 2019; Qi et al. 2019), especially in satellite-based climate monitoring (Awalludin et al. 2024; Muhadi et al. 2020; Hoerer, Bachofer, and Kuenzer 2020) and disaster analysis (Gupta, Watson, and Yin 2021; Pi, Nath, and Behzadan 2021), where occlusions from clouds or shadows often obscure critical surface areas like land, rivers, and infrastructure.

Existing approaches (Tai et al. 2025; Zhan et al. 2024; Ozguroglu et al. 2024; Gao et al. 2023; Xiao et al. 2021; Zhan et al. 2020) typically rely on a single model to predict amodal masks across all object categories and shapes. However, this one-size-fits-all strategy often leads to generic predictions due to limited model capacity, either failing to predict the precise geometry of occluded regions or generating implausible completions, making it difficult to handle complex occlusions and diverse object shapes accurately.

A natural solution to this challenge is to leverage the Mixture of Experts (MoE) (Shazeer et al. 2017; Riquelme et al. 2021) framework, which utilizes multiple specialized experts to better capture the diverse shape variations of target objects. However, routers in existing MoE frameworks often rely on simple softmax-based gating networks that lack an understanding of fine-grained shape semantics. This limitation results in suboptimal routing, where samples are assigned to inappropriate experts specialized in certain shape patterns. Consequently, such mismatches between samples and experts lead to limited performance in the amodal mask prediction. Moreover, the expert design in the existing MoE-based method for amodal instance segmentation (Liu et al. 2025) focuses solely on varying occlusion levels within certain shapes, without explicitly considering the rich diversity of amodal shape variations.

In this paper, we propose ShapeMoE, a novel shape-aware sparse mixture of experts framework tailored for amodal instance segmentation, enabling flexible and efficient learning over highly diverse occluded shapes. The core idea is to model the shape characteristics of each object and route them to the most suitable expert for amodal segmentation. Specifically, our method consists of three key designs. First, we design a shape modeling approach to capture the shape distribution of each object. Specifically, we generate shape-specific embeddings from its visible mask, which serve as

\*Corresponding author.

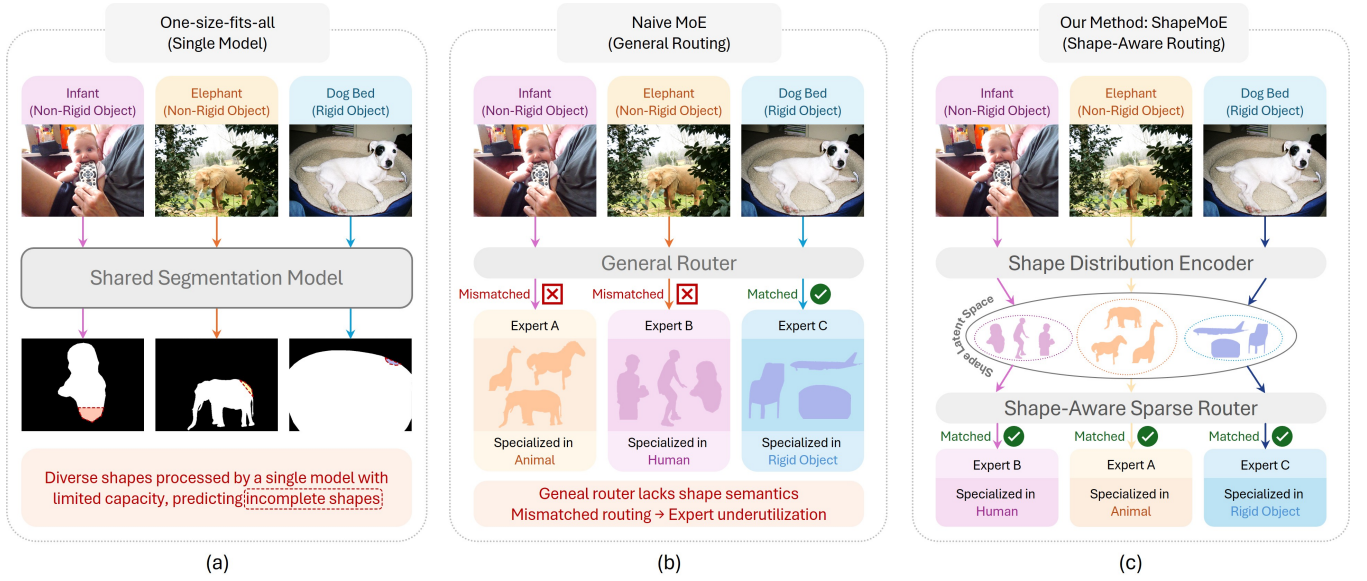


Figure 1: Motivation and Comparison of Routing Strategies. (a) One-size-fits-all models treat all shape types equally, often producing incomplete predictions under occlusion. (b) Naive MoE approaches rely on softmax-based routing without modeling shape distributions, leading to a mismatch between samples and experts. (c) Our ShapeMoE framework encodes each shape as a Gaussian distribution in a latent space, enabling shape-aware sparse routing to specialized experts and improving segmentation of diverse amodal shapes. Best viewed in color.

input prompts for locating the corresponding target object. Assuming that object shapes follow a Gaussian distribution, we estimate the corresponding Gaussian parameters from the shape embeddings to effectively characterize the underlying shape distribution in the latent space. This modeling enables a compact representation of each mask’s geometric identity, effectively capturing shape variations in a latent shape space, while facilitating clear discrimination between different shape patterns.

Next, based on the predicted shape distribution, we present a gating network named Shape-Aware Sparse Router, which routes each sample according to its shape characteristics. Unlike conventional gating mechanisms that compute softmax weights directly from pooled features without explicit shape modeling, our router takes the predicted Gaussian parameters, which characterize the shape distribution, as input and determines the most appropriate expert, ensuring that each sample is processed by an expert specialized in its corresponding shape pattern. Moreover, by leveraging the sparse MoE mechanism (Shazeer et al. 2017), our method achieves high model capacity with various experts while maintaining computational efficiency, as only one expert is activated per sample. Furthermore, our design offers clear interpretability by enabling the statistical analysis and visualization of the shape patterns handled by each expert, revealing their specialization in distinct geometric structures. Crucially, even for unseen objects, their shape embeddings can be projected into the same latent distributional space, enabling the router to effectively assign them to the most suitable expert and allowing the model to generalize beyond the shapes observed during training.

Finally, we introduce a carefully designed shape-specialized segmentation expert to effectively handle diverse occlusion patterns in object shapes. While directly replicating the entire mask decoder architecture, such as that in SAM, is a straightforward way to construct expert branches, it results in substantial computational overhead and redundant capacity. To address this, we first analyze the decoder architecture to identify the components most critical for shape-specific reasoning. Based on this analysis, we selectively convert the compact, shape-sensitive components into multiple expert branches, introducing only marginal additional parameters. Each sample is then routed to the most appropriate expert via our Shape-Aware Sparse Router. This design allows each expert to focus on distinct amodal shape patterns while sharing common visual features, thereby enhancing the model’s capacity to reason about occlusion and capture intrinsic shape diversity.

To summarize, our contributions are threefold. First, we propose ShapeMoE, a sparse mixture-of-experts framework that, to the best of our knowledge, is the first to explicitly model shape diversity and dynamically route each instance to a specialized expert, alleviating the limitations of one-size-fits-all amodal segmentation models. Second, we design a Gaussian-guided routing mechanism that enables interpretable, distribution-based expert assignment within a learned shape embedding space, while naturally generalizing to unseen shapes. Third, we convert lightweight, shape-specific decoder components into multiple expert branches, enabling focused and efficient shape-aware learning with minimal additional cost while improving occlusion handling and capturing diverse object shapes. Finally, we conduct

comprehensive experiments on challenging amodal segmentation datasets, including COCOA, KINS, and D2SA, demonstrating consistent improvements in amodal segmentation, especially the accuracy of occluded regions over state-of-the-art methods.

## 2 Related Work

### 2.1 Amodal Segmentation

Amodal Segmentation (Li and Malik 2016; Zhu et al. 2017) comprises predicting the visible and occluded areas to obtain the complete shape of the target object. Most existing approaches (Xiao et al. 2021; Sun, Kortylewski, and Yuille 2022; Li et al. 2022; Chen et al. 2023; Gao et al. 2023; Li et al. 2023b; Tran et al. 2024; Sun, Kortylewski, and Yuille 2021) explore the usage of shape prior knowledge to enhance the prediction of amodal masks, while some approaches utilize specific designs such as semantics-aware distance map (Zhang et al. 2019), occlusion relationship construction (Zhan et al. 2020; Back et al. 2022; Zheng et al. 2021), boundary uncertainty (Nguyen and Todorovic 2021), occlusion condition modeling (Li et al. 2023a) and multi-view relations learning (Li et al. 2023c).

Recently, with the advancement of large language models (LLMs) and foundation models, several approaches have begun exploring the amodal segmentation task through these powerful paradigms. For example, AURA (Li et al. 2025) presents a novel method and dataset that explores predicting visible and amodal masks by reasoning the implicit intention in the user’s textual input. Zero-shot methods (Liu et al. 2025; Ao et al. 2025) utilize off-the-shelf foundation models to directly predict amodal masks on unseen objects effectively. Moreover, SDAmodal (Zhan et al. 2024) reuses the knowledge of the Stable Diffusion model to generate amodal masks precisely, while SAMEO (Tai et al. 2025) finetunes Efficient-SAM (Xiong et al. 2024) on a synthetic dataset for generalizable amodal segmentation.

Although these methods have achieved notable performance, all of these methods are designed to comprehend the occluded shape and predict amodal masks based on a single model with limited model capacity. To enhance the model learning capacity while keeping efficiency, a novel shape-aware mixture-of-experts framework named VEAL is designed with a sparse paradigm. Based on our ShapeMoE, shape distributions are learned and dynamically assigned with shape-specific experts for predicting amodal masks adaptively.

### 2.2 Mixture-of-Expert Mechanism

Mixture of Experts (MoE) architectures have emerged as a compelling solution to scale model capacity while maintaining computational efficiency. Many approaches (Shazeer et al. 2017; Cai, Gu, and Zhang 2018; Riquelme et al. 2021) have demonstrated how sparse routing can activate only a subset of experts per input, significantly reducing computation without sacrificing performance. The integration of MoE with transformer-based architectures (Lepikhin et al. 2020; Fedus, Zoph, and Shazeer 2022) has further improved

this paradigm, enabling large models with billions of parameters while keeping efficient inference.

However, although directly integrating MoE with amodal segmentation methods can improve the capacity for shape learning, shape characteristics of occluded objects have not been explored in existing MoE frameworks. Considering there are no existing approaches exploring the MoE for shape modeling in the amodal segmentation task at present, we propose ShapeMoE to be aware of the shape distribution of each object to effectively assign objects to shape-specific experts for high-quality amodal segmentation.

## 3 Methodology

In this section, we first introduce the task definition of the targeted problem, and then the overall architecture of our proposed approach is presented. Next, the design for learning shape distribution of each object, the shape-aware sparse routing mechanism for object assignment, and the shape-specialized expert specifically designed to handle occluded objects segmentation for different shapes are presented. Finally, the loss functions used in our method are introduced.

### 3.1 Task Definition

Amodal segmentation task takes an input image  $I$  as input, and optionally takes prompts like visible mask  $M_v$  for locating the target object. The output of a model is the amodal mask  $\hat{M}_a$  of the target object, covering the visible and occluded regions.

### 3.2 Overall Architecture

In this paper, we present the designed ShapeMoE, a shape-aware sparse MoE framework for amodal segmentation. As shown in Fig. 2, the overall architecture of ShapeMoE consists of four stages. (1) The input image  $I$  is fed into the Image Feature Encoder for extracting the general image feature  $F_I$ , while the input visible mask  $M_v$  is embedded by the Mask Embedding Encoder  $\mathcal{E}_M$  for obtaining the mask embedding  $e_m$ , which can be regarded as a feature pointing to the target object. (2) The Shape Distribution Encoder  $\mathcal{E}_S$  takes the mask embedding  $e_m$ , which contains the shape description of the object’s visible region as input, predicting parameters  $\mu$  and  $\sigma$  of a Gaussian distribution representing the shape distribution of the processed object. (3) The Shape-aware Sparse Router  $\mathcal{R}$  then takes the predicted Gaussian parameters  $\mu$  and  $\sigma$  as input and samples a latent shape representation  $l_o$  from the learned distribution. This representation is subsequently used to compute the expert selection scores  $s$ , enabling the assignment of the most suitable expert for each specific shape pattern. (4) Finally, the shape-specialized segmentation expert  $\mathcal{D}$  selected by the router is employed to predict the final segmentation mask, leveraging its specialized knowledge of the assigned shape pattern.

### 3.3 Shape Distribution Learning

To model the shape distribution of the target object, we design a Shape Distribution Encoder  $\mathcal{E}_S$  to learn a probabilistic shape distribution from the mask embedding  $e_m$  predicted

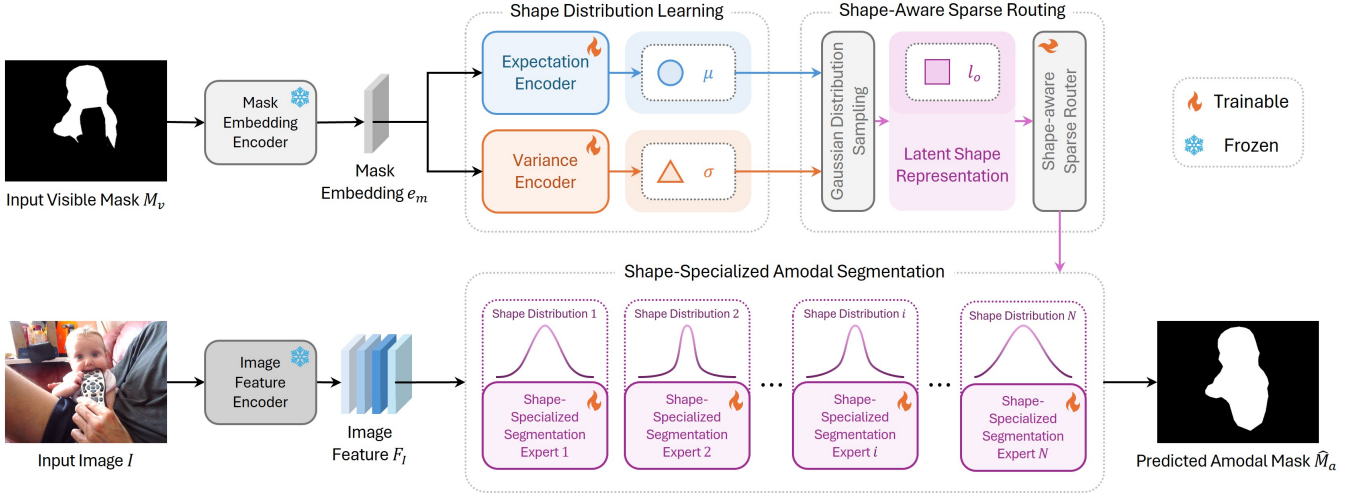


Figure 2: Given an input image and a visible mask, ShapeMoE performs amodal segmentation through the following stages. (1) The image is encoded by the image feature encoder, while the visible mask is embedded into a shape-aware mask embedding. (2) The Shape Distribution Encoder predicts the Gaussian parameters that characterize the object’s shape distribution in a learned latent space. (3) A latent shape representation is sampled, and the Shape-aware Sparse Router computes expert selection scores to route each instance to the most appropriate expert. (4) The selected expert, specialized in specific shape patterns, predicts the final high-quality amodal segmentation mask. Best viewed in color.

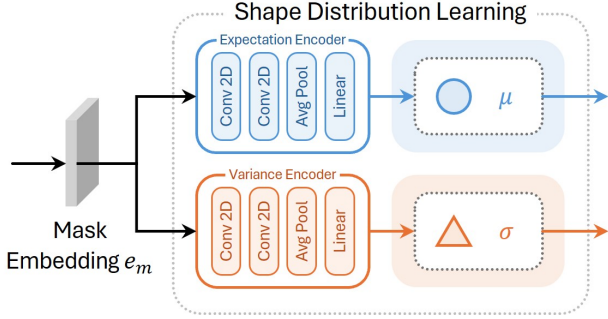


Figure 3: Architecture of the Shape Distribution Encoder.

by the Mask Embedding Encoder  $\mathcal{E}_M$ . As shown in Fig. 3, the object’s amodal shape distribution is assumed to follow a Gaussian distribution  $\mathcal{N}(\mu, \sigma^2)$ . Based on this, two separate encoders, including Expectation Encoder  $\mathcal{E}_\mu$  and Variance Encoder  $\mathcal{E}_\sigma$  contained in the  $\mathcal{E}_S$ , are employed to estimate the mean and standard deviation, respectively:

$$\mu = \mathcal{E}_\mu(e_m), \quad \sigma = \mathcal{E}_\sigma(e_m), \quad (1)$$

where the mean  $\mu$  represents the center of the shape distribution, while the standard deviation  $\sigma$  means the variability or ambiguity of the shape.

The Gaussian parameters ( $\mu$  and  $\sigma$ ) provide a probabilistic representation of shape characteristics, which can be leveraged by the router to effectively guide the expert selection.

### 3.4 Shape-Aware Sparse Routing

We present the shape-aware sparse router  $\mathcal{R}$  to dynamically match between the mask embedding  $e_m$  and the correspond-

ing most suitable experts that specialize in the shape pattern. Specifically, the latent shape representation  $l_o \in \mathbb{R}^d$  capturing the shape pattern of the target object is first sampled from the learned Gaussian distribution  $\mathcal{N}(\mu, \sigma^2)$  with the differentiable reparameterization method inspired by (Qiu et al. 2024). Here  $d$  is the hidden dimension of  $l_o$ . The sampling process can be formulated as follows:

$$l_o = \mu + \text{Softplus}(\sigma) \odot \eta, \quad \eta \sim \mathcal{N}(0, 1) \quad (2)$$

where  $\odot$  denotes element-wise multiplication, and  $\eta$  is sampled from the standard normal distribution as the random noise to improve robustness and model uncertainty. The Softplus function is used to ensure the output is strictly positive while preserving differentiability.

Next, the latent shape representation  $l_o$  is utilized to predict the score  $s \in \mathbb{R}^K$  for  $K$  experts selection as follows:

$$s = W * l_o, \quad (3)$$

where  $W$  is a trainable matrix to transforms the latent shape representation  $l_o$  into expert scores  $s$ , representing the affinity between the sample and experts. During training,  $W$  is optimized via backpropagation, so the model can learn how to route each latent shape representation  $l_o$  to the most appropriate experts.

Finally, to sparsify the routing, we retain the original scores of the top- $k$  experts in  $s$  and set the remaining ones to  $-\infty$ , ensuring zero probability. A softmax is then applied to obtain the routing distribution:

$$\pi = \text{Softmax}(\text{TopK}(s, k)), \quad (4)$$

where  $\pi \in \mathbb{R}^k$  denotes the resulting sparse probability distribution over the selected top- $k$  experts.

It is worth noting that only the top- $k$  selected experts are assigned samples for segmentation, while the unselected experts remain inactive, enabling increased model capacity for shape diversity without sacrificing efficiency.

### 3.5 Shape-Specialized Segmentation Expert

To enable high-quality amodal mask prediction, we introduce a shape-specialized segmentation expert. Given the strong generalization ability of the Segment Anything Model (SAM) (Kirillov et al. 2023), we adopt it as the base framework for implementing our expert design. SAM comprises an Image Feature Encoder for extracting general image features  $F_I$ , a Mask Embedding Encoder for embedding the input prompt, and a mask decoder that predicts segmentation masks based on the image feature and the embedded prompt.

A naive implementation would duplicate the entire mask decoder  $K$  times to instantiate multiple experts. However, this approach is inefficient and suboptimal, as not all components within the decoder contribute equally to shape prediction. Specifically, the two-way Transformer, the first stage of the decoder, is computationally expensive and primarily focuses on generating refined image-level features  $F$  from the Image Feature Encoder output  $F_I$ , without directly contributing to mask generation. In contrast, the second stage, the hyper-network, is lightweight yet directly responsible for producing the mask weights  $w$ , which are subsequently multiplied with  $F$  to generate the final masks. Therefore, this component is explicitly tied to shape reasoning and prediction.

Motivated by this analysis, we take the hyper-network as the core shape-specialized module and replicate it across  $K$  expert branches with only marginal parameter overhead. This targeted design allows each expert to specialize in distinct shape patterns, guided by our Shape-Aware Sparse Router that dynamically assigns each sample to the most appropriate expert for predicting the amodal mask  $\hat{M}_a$ . As a result, our architecture achieves efficient and precise amodal segmentation through focused expert specialization.

### 3.6 Loss Functions

The overall loss function  $\mathcal{L}$  comprises two components: one for supervising the predicted amodal segmentation masks and the other for balancing expert utilization. Specifically, the cross-entropy loss  $\mathcal{L}_{CE}$  is used to supervise the amodal mask prediction, while a Coefficient of Variation Squared ( $CV^2$ ) loss (Shazeer et al. 2017) is employed to encourage balanced expert selection. The overall loss function is defined as:

$$\mathcal{L} = \mathcal{L}_{CE}(\hat{M}_a, M_a) + \mathcal{L}_{CV^2}(\pi), \quad (5)$$

where  $M_a$  denotes the ground-truth amodal mask, and  $\pi$  represents the selection probabilities over experts.

## 4 Experiments

To evaluate the effectiveness of our proposed method, we conduct comprehensive experiments on publicly available amodal segmentation datasets, providing both quantitative

and qualitative results. In addition, we perform extensive ablation studies to validate the contributions of each component in our framework across different aspects.

### 4.1 Datasets

All of our experiments, covering both our method and the compared baselines, are conducted on the following challenging amodal segmentation benchmarks. (1) D2SA (Follmann et al. 2019) is built upon the D2S (Follmann et al. 2018) dataset by augmenting it with high-quality amodal mask annotations. It features a variety of merchandise items placed on a rotatable platform under diverse poses and lighting conditions. This setup closely reflects real-world scenarios such as self-checkout systems in retail environments and warehouse inventory management. The dataset comprises 5,600 images with 28,720 annotated instances across 60 object categories. (2) COCOA-cls (Follmann et al. 2019) is an amodally annotated dataset based on the widely used COCO (Lin et al. 2014) benchmark. It contains 3,501 images and 10,592 object annotations, each with both visible and amodal masks across 80 object categories. COCOA-cls has been widely adopted for evaluation due to its coverage of diverse everyday scenarios, including both indoor and outdoor scenes. (3) KINS (Qi et al. 2019) is an amodal segmentation dataset derived from the KITTI (Geiger, Lenz, and Urtasun 2012) benchmark, primarily focusing on street scenes involving pedestrians and vehicles for autonomous driving applications. It contains 7,474 images in the training set and 7,517 images in the testing set. To ensure fair comparison, all methods are trained and evaluated on the official training and validation sets of each dataset. Ground-truth amodal masks are used for supervision and evaluation.

### 4.2 Implementation Details

Our ShapeMoE framework is implemented in PyTorch (Paszke et al. 2019) and trained using the AdamW optimizer with a batch size of 1. All experiments are performed on a workstation with an NVIDIA RTX 5090 GPU (32 GB), an AMD 9950X3D processor, 96 GB of system memory, and Windows 11 as the operating system. In ShapeMoE, the Image Feature Encoder equipped with an adapter (Chen et al. 2024) is initialized using the pretrained weights of ViT-H (Dosovitskiy et al. 2020). The Mask Embedding Encoder and the shape-specialized segmentation experts are initialized with the weights from SAM2 (Ravi et al. 2024). Remaining parameters in ShapeMoE are randomly initialized (He et al. 2015). No data augmentation techniques are employed.

The evaluation metrics include the mean Intersection over Union (mIoU) for the complete amodal masks and for the occluded regions following (Gao et al. 2023), denoted as mIoU<sub>full</sub> and mIoU<sub>occ</sub>, respectively. All experiments are repeated three times, and the results are averaged to ensure stability and reduce the impact of randomness.

### 4.3 Comparison with State-of-the-art Methods

We compare our proposed ShapeMoE with existing state-of-the-art methods on the validation sets of the COCOA-cls and D2SA datasets, as well as the test set of the KINS

Methods	Venue	COCOA-cls (Val)		D2SA (Val)		KINS (Test)	
		mIoU <sub>full</sub> ↑	mIoU <sub>occ</sub> ↑	mIoU <sub>full</sub> ↑	mIoU <sub>occ</sub> ↑	mIoU <sub>full</sub> ↑	mIoU <sub>occ</sub> ↑
BCNet (Ke, Tai, and Tang 2021)	CVPR 2021	15.10	-	74.90	-	44.00	-
SLN (Zhang et al. 2019)	MM 2019	31.50	-	31.20	-	14.20	-
ORCNN (Follmann et al. 2019)	WACV 2019	57.60	-	74.10	-	55.10	-
Mask-RCNN (He et al. 2017)	ICCV 2017	63.85	-	74.62	-	60.13	-
A3D (Li et al. 2022)	ECCV 2022	64.27	-	74.71	-	61.43	-
GIN (Li et al. 2023b)	TMM 2023	72.46	-	78.23	-	68.31	-
AISFormer (Tran et al. 2022)	BMVC 2022	72.69	13.75	86.81	30.01	81.53	<u>48.54</u>
SAM† (Kirillov et al. 2023)	ICCV 2023	73.10	-	84.65	-	75.88	-
SDXL-Inpainting† (Podell et al. 2024)	ICLR 2024	73.65	-	80.53	-	76.19	-
PCNet (Zhan et al. 2020)	CVPR 2020	76.91	20.34	80.45	28.56	78.02	38.14
VRSP (Xiao et al. 2021)	AAAI 2021	78.98	22.92	88.08	35.17	80.70	47.33
Pix2Gestalt† (Ozguroglu et al. 2024)	CVPR 2024	79.08	-	81.82	-	81.45	-
SDAmodal (Zhan et al. 2024)	CVPR 2024	80.01	-	-	-	-	-
C2F-Seg (Gao et al. 2023)	ICCV 2023	80.28	-	89.10	-	82.22	-
SAMBA† (Liu et al. 2025)	CVPR 2025	81.82	-	90.98	-	88.47	-
<b>ShapeMoE (Ours)</b>	-	<b>89.53</b>	<b>30.68</b>	<b>92.40</b>	<b>37.95</b>	<b>89.82</b>	<b>49.70</b>

Table 1: Comparison on amodal segmentation performance on three datasets, including COCOA-cls, D2SA, and KINS. † denotes a zero-shot method which pretrained on a large-scale amodal segmentation dataset (Ozguroglu et al. 2024). Larger metric values of mIoU<sub>full</sub> and mIoU<sub>occ</sub> indicate better performance. Best performance is in bold for each metric.

dataset. Methods marked with † are zero-shot approaches pretrained on a large-scale synthetic amodal segmentation dataset (Ozguroglu et al. 2024), which contains approximately 870,000 images with amodal annotations. Quantitative and qualitative results are presented in the following.

**Quantitative Results.** As shown in Table 1, we present the quantitative comparison with state-of-the-art methods. ShapeMoE consistently achieves the best performance on the COCOA-cls, D2SA, and KINS datasets across all metrics, including mIoU<sub>full</sub> and mIoU<sub>occ</sub>. Compared to C2F-Seg, the state-of-the-art fully supervised method trained on the same datasets, ShapeMoE surpasses it by 9.25%, 3.3%, and 7.6% on the mIoU<sub>full</sub> metric for COCOA-cls, D2SA, and KINS, respectively. Furthermore, compared to SAMBA, the state-of-the-art zero-shot method, ShapeMoE achieves improvements of 7.71%, 1.42%, and 1.35% on the mIoU<sub>full</sub> metric across the three datasets. This performance gain can be attributed to ShapeMoE’s ability to explicitly model shape distributions and dynamically route each instance to a specialized expert, enabling more accurate and shape-aware amodal mask prediction with larger model capacity.

**Qualitative Results.** Fig. 4 presents qualitative results of the proposed ShapeMoE method on the COCOA-cls dataset. Four representative cases are shown from left to right. ShapeMoE demonstrates strong performance across various occlusion scenarios. For example, in Case 1, the rigid object bench is accurately predicted with a complete amodal mask, despite being partially occluded by the trunk of a tree. In Cases 2 and 4, the human subjects are partially occluded by a baseball bat crossing the body and a camera located within the body region, respectively. ShapeMoE successfully predicts complete amodal masks in both scenarios. In Case 3, although the horse is partially occluded by a human leg,

Index	Total Experts	COCOA-cls	D2SA	KINS
1	1	89.19	91.55	88.15
2	2	89.37	91.58	89.02
3	4	<b>89.53</b>	<b>92.40</b>	<b>89.82</b>
4	8	89.37	90.18	88.66
5	16	89.36	91.42	89.11

Table 2: Ablation on the total number of experts.

ShapeMoE successfully handles the occlusion through the use of shape-specialized experts tailored for complex occlusions, producing a high-quality amodal mask.

#### 4.4 Ablation Study

We conduct ablation studies on the COCOA-cls, D2SA, and KINS datasets to evaluate the effect of key components in ShapeMoE. Specifically, we examine the impact of the total number of experts, which influences the model’s capacity to represent shape diversity. We also vary the number of selected experts per sample to study how routing sparsity affects performance. In addition, we assess the contribution of the expert balancing loss, which helps uniform expert usage.

**Effect of Entire Expert Number.** We investigate how the total number of experts affects segmentation performance, while keeping the selected expert number fixed at 1. As shown in Table 2, increasing the number of experts from 1 to 4 leads to consistent performance improvements across all datasets, indicating that having more specialized experts helps better capture shape diversity. The best results are achieved when using 4 experts. However, further increasing the expert count to 8 or 16 results in performance drops, likely due to expert under-utilization and increased difficulty





Figure 4: Qualitative results of the proposed ShapeMoE. Four representative cases are shown across various object categories, including bench, human, and horse, demonstrating ShapeMoE’s ability to handle complex occlusions and varied amodal shapes. Best viewed in color and zoomed in for details.

Index	Selected Expert Number	COCOA-cls	D2SA	KINS
1	1	<b>89.53</b>	<b>92.40</b>	<b>89.82</b>
2	2	89.46	91.68	89.68
3	3	89.34	91.47	89.70
4	4	89.50	91.39	89.59

Table 3: Ablation on the number of selected experts.

in routing optimization. These results suggest that a moderate number of well-trained experts is sufficient to balance specialization and efficiency.

**Effect of Selected Expert Number.** We evaluate the impact of the number of selected experts per sample while keeping the total number of experts fixed at 4. As shown in Table 3, selecting only one expert per sample achieves the best overall performance, particularly on the COCOA-cls and D2SA datasets. As the number of selected experts increases, performance shows a slight decline. This indicates that sparse expert selection is more effective, as it encourages clear expert specialization and reduces redundancy in computation. These results support the use of sparsely activated expert routing in ShapeMoE.

**Effect of Expert Balancing Loss.** We study the effect of introducing the expert balancing loss, which is designed to encourage uniform utilization of all experts during training. As shown in Table 4, removing the balancing loss leads to consistent performance drops across all three datasets. This

Index	Expert Balancing Loss	COCOA-cls	D2SA	KINS
1		87.61	91.55	88.06
2	✓	<b>89.53</b>	<b>92.40</b>	<b>89.82</b>

Table 4: Ablation on the effect of expert balancing loss.

confirms the importance of maintaining balanced expert usage to ensure stable routing and effective specialization.

## 5 Conclusion

In this paper, we present ShapeMoE, a novel shape-specific sparse Mixture-of-Experts framework designed for amodal instance segmentation. To handle the inherent challenge posed by shape diversity and complex occlusions, ShapeMoE explicitly models the latent shape distribution of each object and dynamically assigns it to a specialized lightweight expert via a Shape-Aware Sparse Router. By encoding object shapes into Gaussian embeddings and leveraging shape-aware routing, ShapeMoE enables each sample to be matched with a specialized expert based on its shape characteristics, leading to more accurate and reliable amodal mask predictions. Extensive experiments demonstrate that ShapeMoE consistently outperforms state-of-the-art methods across multiple datasets, particularly in accurately segmenting heavily occluded regions. In future work, we will explore lightweight segmentation architectures to improve efficiency. We believe our designed shape-aware expert rout-

ing paradigm can offer a promising direction for segmentation under complex occlusions and shape diversity.

## References

- Ao, J.; Jiang, Y.; Ke, Q.; and Ehinger, K. A. 2025. Open-world amodal appearance completion. In *Proceedings of the IEEE/CVF Conference on Computer Vision and Pattern Recognition*, 6490–6499.
- Awalludin, E. A.; Yussof, W.; Bachok, Z.; Aminudin, M. A. F.; Din, M. S. C.; and Hitam, M. S. 2024. Monitoring climate change effects on coral reefs using edge-based image segmentation. *Int. J. Electr. Comput. Eng*, 14: 398–408.
- Back, S.; Lee, J.; Kim, T.; Noh, S.; Kang, R.; Bak, S.; and Lee, K. 2022. Unseen object amodal instance segmentation via hierarchical occlusion modeling. In *International Conference on Robotics and Automation*, 5085–5092. IEEE.
- Cai, J.; Gu, S.; and Zhang, L. 2018. Learning a deep single image contrast enhancer from multi-exposure images. *IEEE Transactions on Image Processing*, 27(4): 2049–2062.
- Chen, J.; Niu, L.; Zhang, J.; Si, J.; Qian, C.; and Zhang, L. 2023. Amodal instance segmentation via prior-guided expansion. In *Proceedings of the AAAI Conference on Artificial Intelligence*, volume 37, 313–321.
- Chen, T.; Lu, A.; Zhu, L.; Ding, C.; Yu, C.; Ji, D.; Li, Z.; Sun, L.; Mao, P.; and Zang, Y. 2024. Sam2-adapter: Evaluating & adapting segment anything 2 in downstream tasks: Camouflage, shadow, medical image segmentation, and more. *arXiv preprint arXiv:2408.04579*.
- Dosovitskiy, A.; Beyer, L.; Kolesnikov, A.; Weissenborn, D.; Zhai, X.; Unterthiner, T.; Dehghani, M.; Minderer, M.; Heigold, G.; Gelly, S.; et al. 2020. An image is worth 16x16 words: Transformers for image recognition at scale. *arXiv preprint arXiv:2010.11929*.
- Fedus, W.; Zoph, B.; and Shazeer, N. 2022. Switch transformers: Scaling to trillion parameter models with simple and efficient sparsity. *Journal of Machine Learning Research*, 23(120): 1–39.
- Follmann, P.; Bottger, T.; Hartinger, P.; König, R.; and Ulrich, M. 2018. MVTec D2S: densely segmented supermarket dataset. In *Proceedings of the IEEE/CVF European Conference on Computer Vision*, 569–585.
- Follmann, P.; König, R.; Härtinger, P.; Klostermann, M.; and Böttger, T. 2019. Learning to see the invisible: End-to-end trainable amodal instance segmentation. In *Proceedings of the IEEE/CVF Winter Conference on Applications of Computer Vision*, 1328–1336. IEEE.
- Gao, J.; Qian, X.; Wang, Y.; Xiao, T.; He, T.; Zhang, Z.; and Fu, Y. 2023. Coarse-to-fine amodal segmentation with shape prior. In *Proceedings of the IEEE/CVF International Conference on Computer Vision*, 1262–1271.
- Geiger, A.; Lenz, P.; and Urtasun, R. 2012. Are we ready for autonomous driving? the KITTI vision benchmark suite. In *Proceedings of the IEEE/CVF Conference on Computer Vision and Pattern Recognition*, 3354–3361. IEEE.
- Gupta, A.; Watson, S.; and Yin, H. 2021. Deep learning-based aerial image segmentation with open data for disaster impact assessment. *Neurocomputing*, 439: 22–33.
- He, K.; Gkioxari, G.; Dollár, P.; and Girshick, R. 2017. Mask R-CNN. In *Proceedings of the IEEE/CVF International Conference on Computer Vision*, 2961–2969.
- He, K.; Zhang, X.; Ren, S.; and Sun, J. 2015. Delving deep into rectifiers: Surpassing human-level performance on imagenet classification. In *Proceedings of the IEEE/CVF International Conference on Computer Vision*, 1026–1034.
- Hoeser, T.; Bachofer, F.; and Kuenzer, C. 2020. Object detection and image segmentation with deep learning on Earth observation data: A review—Part II: Applications. *Remote Sensing*, 12(18): 3053.
- Ke, L.; Tai, Y.-W.; and Tang, C.-K. 2021. Deep occlusion-aware instance segmentation with overlapping bilayers. In *Proceedings of the IEEE/CVF conference on computer vision and pattern recognition*, 4019–4028.
- Kirillov, A.; Mintun, E.; Ravi, N.; Mao, H.; Rolland, C.; Gustafson, L.; Xiao, T.; Whitehead, S.; Berg, A. C.; Lo, W.-Y.; et al. 2023. Segment Anything. In *Proceedings of the IEEE/CVF International Conference on Computer Vision*, 4015–4026.
- Lee, S.-Y.; Jeon, J.-S.; and Le, T. H. M. 2023. Feasibility of automated black ice segmentation in various climate conditions using deep learning. *Buildings*, 13(3): 767.
- Lepikhin, D.; Lee, H.; Xu, Y.; Chen, D.; Firat, O.; Huang, Y.; Krikun, M.; Shazeer, N.; and Chen, Z. 2020. Gshard: Scaling giant models with conditional computation and automatic sharding. *arXiv preprint arXiv:2006.16668*.
- Li, K.; and Malik, J. 2016. Amodal instance segmentation. In *Proceedings of the IEEE/CVF European Conference on Computer Vision*, 677–693. Springer.
- Li, Z.; Shi, R.; Huang, T.; and Jiang, T. 2023a. OAFormer: Learning occlusion distinguishable feature for amodal instance segmentation. In *International Conference on Acoustics, Speech, and Signal Processing*, 1–5. IEEE.
- Li, Z.; Ye, W.; Jiang, T.; and Huang, T. 2022. 2D amodal instance segmentation guided by 3D shape prior. In *Proceedings of the IEEE/CVF European Conference on Computer Vision*, 165–181. Springer.
- Li, Z.; Ye, W.; Jiang, T.; and Huang, T. 2023b. GIN: Generative invariant shape prior for amodal instance segmentation. *IEEE Transactions on Multimedia*.
- Li, Z.; Ye, W.; Terven, J.; Bennett, Z.; Zheng, Y.; Jiang, T.; and Huang, T. 2023c. MUVA: A new large-scale benchmark for multi-view amodal instance segmentation in the shopping scenario. In *Proceedings of the IEEE/CVF International Conference on Computer Vision*, 23504–23513.
- Li, Z.; Yoon, H.; Lee, S.; and Lin, W. 2025. Unveiling the Invisible: Reasoning Complex Occlusions Amodally with AURA. In *Proceedings of the IEEE/CVF International Conference on Computer Vision*.
- Lin, T.-Y.; Maire, M.; Belongie, S.; Hays, J.; Perona, P.; Ramanan, D.; Dollár, P.; and Zitnick, C. L. 2014. Microsoft coco: Common objects in context. In *Proceedings of the IEEE/CVF European Conference on Computer Vision*, 740–755. Springer.



- Liu, Z.; Qiao, L.; Chu, X.; Ma, L.; and Jiang, T. 2025. Towards Efficient Foundation Model for Zero-shot Amodal Segmentation. In *Proceedings of the IEEE/CVF Conference on Computer Vision and Pattern Recognition*, 20254–20264.
- Muhadi, N. A.; Abdullah, A. F.; Bejo, S. K.; Mahadi, M. R.; and Mijic, A. 2020. Image segmentation methods for flood monitoring system. *Water*, 12(6): 1825.
- Nguyen, K.; and Todorovic, S. 2021. A weakly supervised amodal segmenter with boundary uncertainty estimation. In *Proceedings of the IEEE/CVF International Conference on Computer Vision*, 7396–7405.
- Ozguroglu, E.; Liu, R.; Surís, D.; Chen, D.; Dave, A.; Tokmakov, P.; and Vondrick, C. 2024. pix2gestalt: Amodal Segmentation by Synthesizing Wholes. *Proceedings of the IEEE/CVF Conference on Computer Vision and Pattern Recognition*.
- Paszke, A.; Gross, S.; Massa, F.; Lerer, A.; Bradbury, J.; Chanan, G.; Killeen, T.; Lin, Z.; Gimelshein, N.; Antiga, L.; et al. 2019. Pytorch: An imperative style, high-performance deep learning library. *Advances in Neural Information Processing Systems*, 32.
- Pi, Y.; Nath, N. D.; and Behzadan, A. H. 2021. Detection and semantic segmentation of disaster damage in UAV footage. *Journal of Computing in Civil Engineering*, 35(2): 04020063.
- Podell, D.; English, Z.; Lacey, K.; Blattmann, A.; Dockhorn, T.; Müller, J.; Penna, J.; and Rombach, R. 2024. Sdxl: Improving latent diffusion models for high-resolution image synthesis. *International Conference on Learning Representations*.
- Qi, L.; Jiang, L.; Liu, S.; Shen, X.; and Jia, J. 2019. Amodal instance segmentation with KINS dataset. In *Proceedings of the IEEE/CVF Conference on Computer Vision and Pattern Recognition*, 3014–3023.
- Qiu, X.; Wu, X.; Lin, Y.; Guo, C.; Hu, J.; and Yang, B. 2024. Duet: Dual clustering enhanced multivariate time series forecasting. *arXiv preprint arXiv:2412.10859*.
- Ravi, N.; Gabeur, V.; Hu, Y.-T.; Hu, R.; Ryali, C.; Ma, T.; Khedr, H.; Rädle, R.; Rolland, C.; Gustafson, L.; et al. 2024. Sam 2: Segment anything in images and videos. *arXiv preprint arXiv:2408.00714*.
- Riquelme, C.; Puigcerver, J.; Mustafa, B.; Neumann, M.; Jenatton, R.; Susano Pinto, A.; Keysers, D.; and Houlsby, N. 2021. Scaling vision with sparse mixture of experts. *Advances in Neural Information Processing Systems*, 34: 8583–8595.
- Shazeer, N.; Mirhoseini, A.; Maziarz, K.; Davis, A.; Le, Q.; Hinton, G.; and Dean, J. 2017. Outrageously large neural networks: The sparsely-gated mixture-of-experts layer. *arXiv preprint arXiv:1701.06538*.
- Sun, Y.; Kortylewski, A.; and Yuille, A. 2021. Weakly-supervised amodal instance segmentation with compositional priors. *International Conference on Learning Representations*.
- Sun, Y.; Kortylewski, A.; and Yuille, A. 2022. Amodal segmentation through out-of-task and out-of-distribution generalization with a Bayesian model. In *Proceedings of the IEEE/CVF Conference on Computer Vision and Pattern Recognition*, 1215–1224.
- Tai, W.-E.; Shih, Y.-L.; Sun, C.; Wang, Y.-C. F.; and Chen, H.-T. 2025. Segment Anything, Even Occluded. In *Proceedings of the IEEE/CVF Conference on Computer Vision and Pattern Recognition*, 29385–29394.
- Tran, M.; Bounsavy, W.; Vo, K.; Nguyen, A.; Nguyen, T.; and Le, N. 2024. ShapeFormer: Shape Prior Visible-to-Amodal Transformer-based Amodal Instance Segmentation. *arXiv preprint arXiv:2403.11376*.
- Tran, M.; Vo, K.; Yamazaki, K.; Fernandes, A.; Kidd, M.; and Le, N. 2022. Aisformer: Amodal instance segmentation with transformer. *British Machine Vision Conference*.
- Xiao, Y.; Xu, Y.; Zhong, Z.; Luo, W.; Li, J.; and Gao, S. 2021. Amodal segmentation based on visible region segmentation and shape prior. In *Proceedings of the AAAI Conference on Artificial Intelligence*, volume 35, 2995–3003.
- Xiong, Y.; Varadarajan, B.; Wu, L.; Xiang, X.; Xiao, F.; Zhu, C.; Dai, X.; Wang, D.; Sun, F.; Iandola, F.; et al. 2024. EfficientSAM: Leveraged masked image pretraining for efficient segment anything. In *Proceedings of the IEEE/CVF Conference on Computer Vision and Pattern Recognition*, 16111–16121.
- Zhan, G.; Zheng, C.; Xie, W.; and Zisserman, A. 2024. Amodal Ground Truth and Completion in the Wild. *Proceedings of the IEEE/CVF Conference on Computer Vision and Pattern Recognition*.
- Zhan, X.; Pan, X.; Dai, B.; Liu, Z.; Lin, D.; and Loy, C. C. 2020. Self-supervised scene de-occlusion. In *Proceedings of the IEEE/CVF Conference on Computer Vision and Pattern Recognition*, 3784–3792.
- Zhang, Z.; Chen, A.; Xie, L.; Yu, J.; and Gao, S. 2019. Learning semantics-aware distance map with semantics layering network for amodal instance segmentation. In *ACM International Conference on Multimedia*, 2124–2132.
- Zheng, C.; Dao, D.-S.; Song, G.; Cham, T.-J.; and Cai, J. 2021. Visiting the invisible: Layer-by-layer completed scene decomposition. *International Journal of Computer Vision*, 129: 3195–3215.
- Zhu, Y.; Tian, Y.; Metaxas, D.; and Dollár, P. 2017. Semantic amodal segmentation. In *Proceedings of the IEEE/CVF Conference on Computer Vision and Pattern Recognition*, 1464–1472.